Analysis of Static Stress in a Bicycle Chain Plate

Maximilian Wagner[1], Thorsten Koch[2], Ingo Kuehne[3], and Alexander Frey*[1]
[1]University of Applied Sciences, Augsburg, Germany, [2]Comsol Multiphysics GmbH, Göttingen, Germany, [3] Heilbronn University, Kuenzelsau, Germany
*Corresponding author: An der Hochschule 1, 86161 Augsburg, Germany, alexander.frey@hs-augsburg.de

Abstract: Using the *Solid Mechanics* application mode a model is setup to investigate the impact of static stress on a bicycle chain for different geometries related to three chain generations. A contact model is used to induce the stress. Plastic deformation is taken into account. Based on the simulation results the contribution of plastic deformation to lifetime restriction can be estimated. The results suggest that common high tension carbon steel can still be used even for increasing stress levels.

Keywords: chain, stress, plasticity, contact.

1. Introduction

Bicycles are popular and inexpensive means of transportation. E.g. in Germany there are 1.84 bicycles per household and 9 % of all transportation is accomplished by bicycle [1].

The chain drive is an essential component for efficient operation. A well designed chain enables an efficiency of 98 % [2]. Beside the efficiency the chain reliability and durability are essential [3]. With increasing number of sprockets in a cassette the chain dimensions have to be adjusted (cf. Fig. 1, 2 and Tab. 1). In this work the impact of the geometrical scaling on the mechanical stress is investigated. Smaller chains result in a smaller thickness of the plates. The resulting increase of mechanical stress for this critical component is analyzed for the 8-, 9- and 10-speed chains shown in Fig. 1.

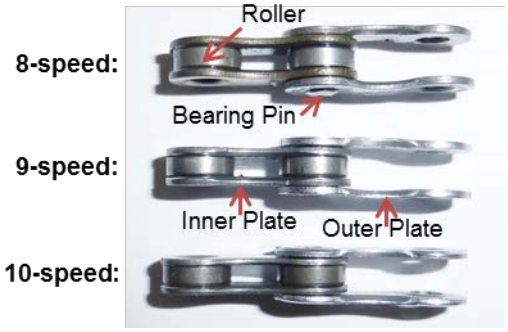

Figure 1. Three chain generations with components.

2. Load Case

The stress analysis requires the definition of the considered load case. It is determined by the applied chain force for varied geometries. Both aspects are specified in the following subsections.

2.1 Chain Geometry

The geometry of the chain is completely characterized with the parameters shown in Fig. 2. Specific values for the considered chain variants of Fig. 1 are summarized in Tab. 1. The chain pitch P and the pin diameter D_i are fixed for all considered chains. However, decreasing dimensions for the outer and inner chain width, B and b, result in a thinner value for the plate thickness T.

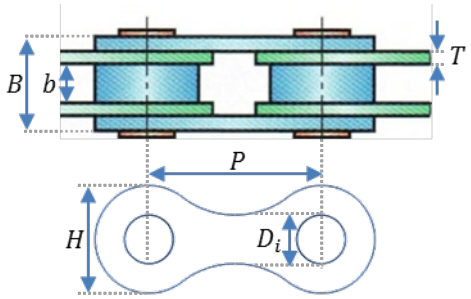

Figure 2. Chain geometry, top view [2]: outer width B, inner width b, plate thickness T and side view: pitch P, pin diameter D_i, plate height H.

Table 1: Geometry parameters (cf. Fig. 2)
[1)] measured; [2)] specified values: $3/32" = 2.38\ mm$, $11/128" = 2.18\ mm$; [3)] values from [4];
[4)] new chain pitch $1/2" = 12.7\ mm$ [4].

Chain Type	$B^{1)}$ *[mm]*	$b^{2)}$ *[mm]*	$T^{1)}$ *[mm]*	$H^{1)}$ *[mm]*	$D_i^{3)}$ *[mm]*	$P^{4)}$ *[mm]*
8s	6.70	2.38	1.06	8.38	3.60	12.7
9s	6.10	2.18	0.96	7.96	3.60	12.7
10s	5.82	2.18	0.82	7.96	3.60	12.7

2.2 Chain Force

The chain force is derived by considering the situation in the drive train shown in Fig. 3. The bicycle rider provides the pedal force F_p. The component F_t is acting perpendicular to the crank of length r_{cr} and creates a torque. This torque has to be balanced by the chain force F_{ch} acting on the sprocket radius r_{sp}. The maximum chain force results for horizontal orientation of the crank ($F_{t,max} = F_p$) and balance requires:

$$F_{t,max} \cdot r_{cr} = F_p \cdot r_{cr} = F_{ch} \cdot r_{sp}. \qquad (1)$$

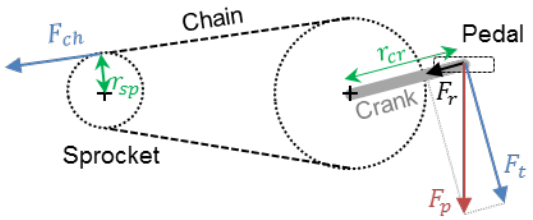

Figure 3. Drivetrain with relevant forces and geometry.

A common crank length is $r_{cr} = 170\ mm$ [2]. The sprocket radius r_{sp} depends on the number of teeth N_{te} (= 22 for minimal sprocket) and the chain pitch P (= 12.7 mm) as [2]:

$$r_{sp} = \frac{N_{te} \cdot P}{2\pi} \qquad (2)$$

According to DIN EN 14764 the crank has to be designed for a maximum force of:

$$F_p = F_{p,max} = 1500\ N \qquad (3)$$

Combining Eqs. (1) – (3) and using the parameters given above result in:

$$F_{ch} = 2\pi \cdot \frac{F_p \cdot r_{cr}}{N_{te} \cdot P} = 5734\ N\ . \qquad (4)$$

3. Simulation Model

The model is setup based on the *Solid Mechanics* application mode. For numeric efficiency a 2D quarter geometry of the plate is used with the plane stress approximation (no stress in direction of thickness T).

3.1 Boundary Conditions

In Fig. 4 all applied boundary conditions are summarized. The quarter geometry requires a *Symmetry* and a *Roller* condition on the boundaries indicated in Fig. 4.

The plate stress is induced by the x-component of the *Body Load* according to:

$$F_{BL,x} = -\frac{F_{ch,max}}{4} \cdot load\_factor(para). \qquad (5)$$

The factor $1/4$ occurs because: first, the chain force is divided between the inner and outer plate (cf. Fig 1) and second, the quarter geometry. The $load\_factor(para)$ in Eq. (5) is displayed in Fig. 5. It results in force ramping and thereby ensures numeric stability for the nonlinear contact simulation (cf. subsection 3.2). Depending on the $para$-range it also allows for cyclic loads (two cycles in case of configuration in Fig. 5).

Finally, there is also a *Spring Foundation* at the point shown in Fig. 4. This is required to have a well-defined problem for the initial case without applied load.

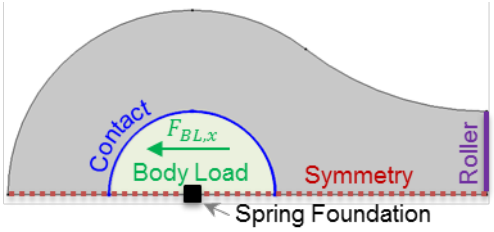

Figure 4. Boundary conditions for the 2D quarter geometry.

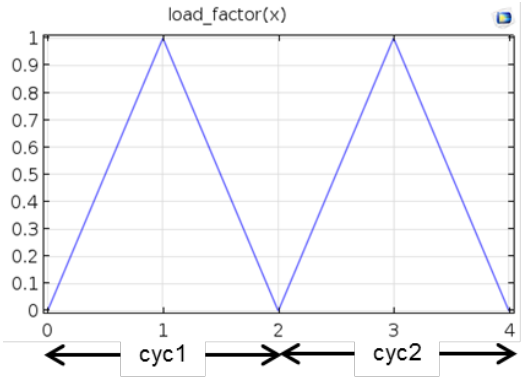

Figure 5. Analytic function $load\_factor(x = para)$ for two load cycles *cyc1* and *cyc2*.

3.2 Contact Modelling

The bearing pin is used to apply the load to the plate. Contact modelling is employed. As shown in Fig. 6, the mesh on the destination side is chosen two times smaller compared to the source (concave) side according to the guide lines in [5] for improving stability.

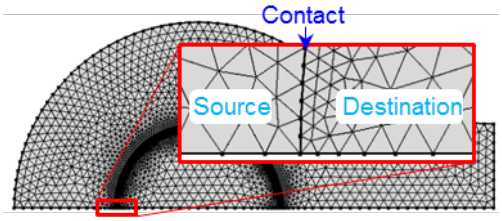

Figure 6. Contact mesh.

Moreover, for stability reasons a spring foundation is established (cf. Fig. 4). It is configured as *force as function of extension* with:

$$k_s \cdot solid.uspring1\_spf1 \cdot spring\_fac(para)$$

with $solid.uspring1\_spf1$ being the x-component of the local spring extension, k_s is the spring constant and $spring\_fac(para)$ is an analytic function (cf. Fig 7) to enable the force only in the proximity of the otherwise critical state (if no body load is applied).

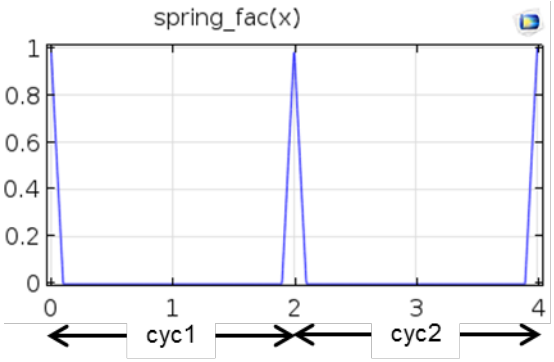

Figure 7. Analytic function $sping\_fac(x = para)$ for two load cycles *cyc1* and *cyc2*.

3.3 Plasticity Modelling

In order to model plasticity the according sub-node below *Linear Elastic Material* is enabled as shown in Fig. 8. The chosen node configuration is summarized in Fig. 9.

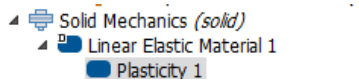

Figure 8. Plasticity physics node

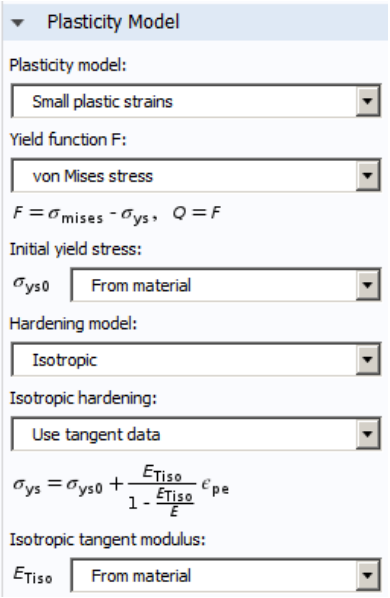

Figure 9. Plasticity node configuration.

3.4 Material Data

In order to model plasticity, initial yield stress data is essential (cf. Fig. 9). For steel it ranges from approximately 300 MPa to over 1700 MPa [6]. Chain Manufacturers do not publish material data. However, in [7] the use of high tension carbon steel, nickel-plated for the plate is reported. Accordingly, 36NiCrMo16 would be a candidate and is used in this work. In Tab. 2 the used material data from [8] is summarized. All other required data is derived from that information.

Table 2: Plate material 36NiCrMo16 data [8]:

Property	Symbol	Value
Young's modulus	E	208 GPa
Shear modulus	G	80 GPa
Initial yield stress (quench and temper condition EN 10083 3:2006)	σ_{ys0}	1050 MPa
Density	ϱ	7840 kg/m^3

The Poisson's ratio ν is calculated with the data of Tab. 2 as:

$$\nu = \frac{E}{2G} - 1 = 0.3. \qquad (6)$$

The setup in Fig. 9 also requires an anisotropic tangent modulus E_{Tiso}. The plastic deformation will increase for smaller values of E_{Tiso}. To avoid underestimation of plastic deformation the value is conservatively chosen as:

$$E_{Tiso} = 0.01\, E = 2080\, MPa. \qquad (7)$$

4. Simulation Results

In the following, the main results are basically displayed. A more detailed discussion follows in section 5.

Simulated *von Mises Stress* (*Gauss-point evaluation*) for the 9-speed chain geometry is shown in Fig. 10. The upper diagram corresponds to the peak load within the second cycle (cf. Fig. 5: $para = 3$). The lower diagram displays the situation at the end of the cycle (cf. Fig. 5: $para = 4$).

Fig. 11 shows examples of simulated *effective plastic strain* for the 9-speed chain geometry. Again, the upper diagram corresponds to the peak load within the second cycle, while the lower diagram displays the situation after relieve at the end of the cycle.

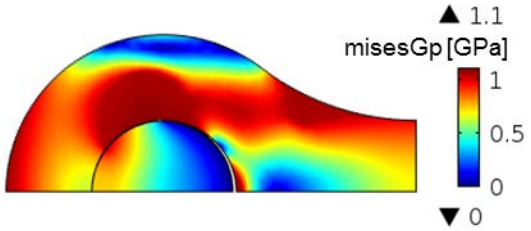

(a)

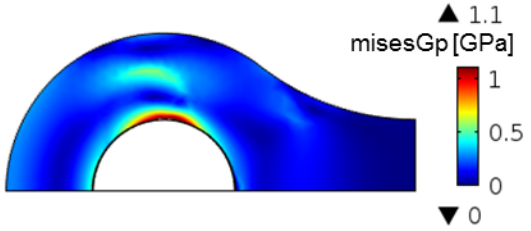

(b)

Figure 10. von Mises Stress, Gauss-point evaluation for 9s-geometry at (a) peak load and (b) after relieve at the end of cycle 2. For cycle definition cf. Fig. 5.

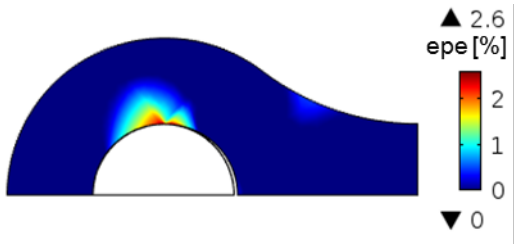

(a)

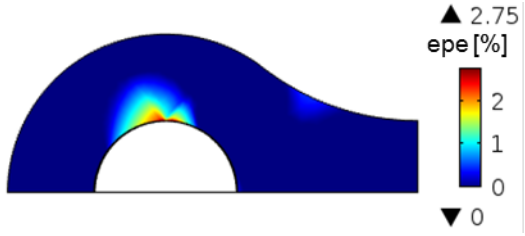

(b)

Figure 11. Effective plastic strain for 9s-geometry at (a) peak load and (b) after relieve at the end of cycle 2. For cycle definition cf. Fig. 5.

The simulated force-displacement characteristics are shown in Fig. 12. The displayed data refer to the full geometry and total chain force and are core results of this work. Once more, two load cycles are applied and the according curves are shown for all investigated chain generations (8-, 9-, 10-speed). Data for the first cycle are drawn with colored solid lines, while the second cycle data is indicated by dotted black lines. In all cases the second cycle data falls together with the relieve path of the first cycle data. Therefore, a third load cycle would not cause a different situation.

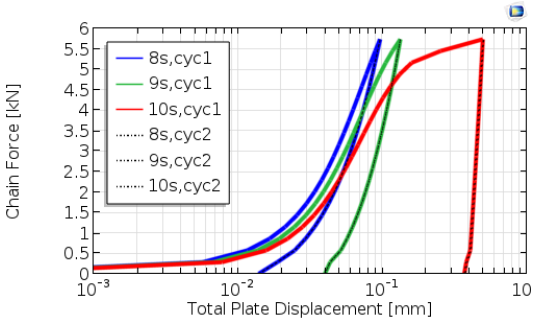

Figure 12. Force-displacement curves for all considered chain variants 8s, 9s and 10s (cf. Tab. 1) for two load cycles.

The permanent plate elongation caused by the effective plastic strain is concluded from Fig. 12. In particular the 10-speed chain experiences an elongation which exceeds an acceptable level (more discussion in section 5). Motivated by this, a parameter study for increased initial yield stress is performed. In this case parameters are taken from [8] for temper conditions other than the one given in Tab. 2. Fig. 13 summarizes the results for the 10-speed geometry.

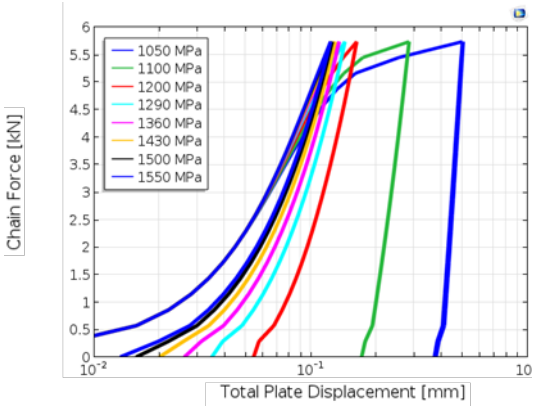

Figure 13. Force-displacement curves for 10s-geometry (cf. Tab. 1) for varied initial yield stress σ_{ys0} (values shown in the legend and taken from [8]).

5. Discussion

One main aspect of this work is the evaluation of the lifetime reduction by static stress. A chain should be changed if the wear measurement per plate reaches 75 µm [2]. From Fig. 12 it is seen that approximately 15 % for 8-speed, 50 % for 9-speed and 500 % for 10-speed of this value is reached. Besides the plastic deformation considered in this work, there are additional mechanisms for chain elongation as fatigue and material removal. Taking that in consideration the result for 8-speed is acceptable, for 9-speed it is marginal and clearly for 10-speed it is unrealistic.

However, based on the parametric initial yield stress study it turns out, that with the appropriate selection of common high tension carbon steel (in this work 36NiCrMo16) reasonable performance is achieved. Referring to Fig. 13 it is possible to reduce the elongation to acceptable 26 % for the 10-speed geometry in case of steel with 1430 MPa initial yield stress.

6. Conclusions

Using the *Solid Mechanics* application mode it was possible to setup a model to analyze the impact of static stress on bicycle chains with varied geometries related to three chain technology generations.

The obtained results suggest that common high tension carbon steel can still be used even for increasing stress levels caused by the scaled geometries. This can be concluded with respect to the plastic deformation.

7. References

[1] Andrea Huetter, *Verkehr auf einen Blick*, Statistisches Bundesamt, Wiesbaden (2013)

[2] Michael Gressmann, *Fachkunde Fahrrad-technik*, Europa-Lehrmittel, Haan-Gruiten (2011)

[3] Shoji Noguchi et al., Static Stress Analysis of Link Plate of Roller Chain using Finite Element Method and Some Design Proposals for Weight Saving, *Journal of Advanced Mechanical Design Systems and Manufacturing*, **Vol.3**, No. 2,(2009)

[4] Fachausschuss Technik des ADFC. *Fahrrad-kette*. Available from: <http://www.fa-technik.adfc.de/Komponenten/Kette/>. [25 July 2015].

[5] *Improve the stability of your contact model*, Available from: <https://www.comsol.de/support/knowledgebase/1102/>. [27 July 2015]

[6]. E.J. Pavlina, C.J. Van Tyne, Correlation of Yield Strength and Tensile Strength with Hardness for Steels, *Journal of Materials Engineering and Performance*, **Vol. 17**, No. 6, pp. 888-893 (2008)

[7] Rohloff, *S-L-T 99 – Technical Information*, Available from: <http://www.rohloff.de/en/technology/chaindrive/s_l_t_99/index.html>. [29 July 2015]

[8] Lucefin Group, *36NiCrMo16 – Technical card*,Available from: <http://www.lucefin.com/wp-content/files_mf/1536nicrmo1662.pdf. [29 July 2015]